Hindawi
Geofluids
Volume 2023, Article ID 5042768, 15 pages
https://doi.org/10.1155/2023/5042768

Research Article

Diagenetic Evolution of Marine Carbonate Reservoirs: A Case Study from $M5_{1-2}$ Submember of Middle Ordovician Majiagou Formation in SE Ordos Basin, China

Haiyan Wu,[1,2] **Ting Liang**,[1] **Chao Gao**,[2] **Yanjun Wu**,[3] **Hongxia Cao**,[2] **Jun Yu**,[2] **Fenfei Bai**,[2] **Jianbo Sun**,[2] **Keyong Li**,[4] **and Yanqin Guo**[5]

[1]*School of Earth Science and Resources, Chang'an University, Xi'an, China*
[2]*Research Institute of Yanchang Petroleum (Group) Co., Ltd., Xi'an, China*
[3]*School of Petroleum and Environmental Engineering, Yan'an University, Yan'an, China*
[4]*College of Geology and Environment, Xi'an University of Science and Technology, Xi'an, China*
[5]*School of Earth Science and Engineering, Xi'an Shiyou University, Xi'an, China*

Correspondence should be addressed to Ting Liang; liangt@chd.edu.cn

Received 11 April 2022; Revised 21 October 2022; Accepted 28 November 2022; Published 18 February 2023

Academic Editor: Dengke Liu

In the Yan'an gas field, southeast of Ordos Basin, the discovered natural gas reserves are 114 billion cubic meters. Highly productive gas reservoirs were formed in paleokarst. By using 164 samples from 27cores, the geochemical study of diagenetic evolution was carried out, and the relationship between different diagenesis environments was discussed by using scanning electron microscopy, carbon and oxygen isotope, and isotopic and fluid inclusion microthermometric observations. Results show that the lithology of reservoir is anhydrite-bearing mud powder crystal dolomite, powder crystal dolomite, and karst breccia dolomite; the filling includes dolomite, calcite, anhydrite, quartz, fluorite, and clay minerals; $\delta^{13}C$ (‰ PDB) value is between −6.31‰ and 1.01‰, $\delta^{18}O$ (‰ PDB) value ranges from −11.36‰ to −6.54‰, and the $^{87}Sr/^{86}Sr$ value ranges from 0.7077 to 0.7081. The overall carbon isotope of Majiagou Formation decreases first and then increases, and the strontium isotope evolution curve generally increases first and then decreases, indicating that the water environment of Majiagou Formation experienced a relatively high salinity concentration period and a relative desalinization period during deposition. The stratigraphic development shows a cyclical trend, responding to the multistage transgression and regression process. The homogenization temperature of fluid inclusions is 70–100°C, salinity is 0–3.5%, homogenization temperature of fluid inclusions is 70–100°C, salinity is >3.5%, homogenization temperature of fluid inclusions is 100–160°C, salinity is 0–3.5%, homogenization temperature of fluid inclusions is 100–160°C, salinity is >3.5%, homogenization temperature of fluid inclusion temperature is 160–200°C, and salinity is >3.5%, indicating that the fluid source in the sedimentation and diagenesis process is seawater, atmospheric freshwater, hydrocarbon fluid, and deep thermal fluid. The diagenetic environments are divided into marine diagenetic environments, metric freshwater diagenetic environments, and burial diagenetic environments.

1. Introduction

Marine carbonate reservoir is an important field of oil and gas accumulation [1–6], such as Tahe, Puguang, Weiyuan, and Jingbian which have been discovered in the exploration [7–10]. In recent years, the exploration system of Ordovician marine carbonate reservoirs in the Ordos Basin has achieved fruitful results [11, 12], in which the Yan'an gas field with discovered natural gas reserves of 114.436 billion square was found in the southeast of Yishan slope. Formation and distribution of marine carbonate rocks are controlled by tectonics, geomorphology, climate, and physiochemical conditions of water [13–20]. Diagenesis history covers the whole process of deposition and burial. Many research evidences show that the activities of various diagenetic fluids affect the pore space morphology of carbonate reservoir closely

[20–30]. Diagenetic environment and diagenesis are important factors controlling reservoir distribution. Sequence boundaries at all levels control the migration of diagenetic fluids in different diagenetic environments. With the development of diagenesis, various forms of pores formed. The evolution of pores, caves, and fractures is a key problem in the study of marine carbonate reservoirs. The dissolution and filling of these are essentially a physical and chemical process between fluid and rock. During the long diagenetic process, the temperature and pressure, minerals, hydrochemical properties, fluid dynamics, and other conditions are different in different diagenetic stages. The alteration, dissolution, precipitation, and porosity change in the reservoir are quite different [31]. Many studies have shown that the Ordovician weathering crust reservoir in Ordos Basin is an ancient structural pattern with high in the middle and low in the east and west during Ordovician, which controls the development of gypsum-bearing dolomite flat in the basin margin and lays a foundation for the development of ancient karst cave reservoirs. Diagenesis during supergene and burial stages has played a stereotype role in the evolution of porosity in paleokarst reservoirs [30–33]. At present, the research on the western and northern parts of the basin is relatively mature. Whether the pore development law of Ordovician carbonate reservoir in the middle and eastern part of the basin is consistent still lacks relevant systematic research.

It is of great significance to identify the types and sources of diagenetic fluids and study the evolution of diagenetic environment for the next exploration of Yan'an gas field in Ordos Basin. Upon sampling of Ordovician carbonate reservoir in more than 20 wells in Yan'an gas field, different types of diagenetic fluids are distinguished and classified by thin section cathodoluminescence observation, fluid inclusion system analysis, and stable isotope analysis and discussion on reservoir reconstruction mechanism, understanding the relationship between diagenetic fluid activity and diagenetic environment evolution.

2. Geological Setting

The Ordos Basin is the second largest oil-and-gas-bearing basin in China covering an area of nearly 370,000 km^2. The basin is bounded by the Yinshan Mountains to the north, the Qinglin Mountains to the south, the Liupan-Helan Mountains to the west, and the Luliang Mountains to the east. The basin is generally rectangular in the north and south (Figure 1).

The basement of Ordos Basin is the crystalline basement of Archean-Palaeoproterozoic, and two large uplifts are developed at the top, namely, the northern Iraq Zhaomeng uplift and the central paleouplift in the central and southern parts. The two uplifts formed an "L" shape in plane, which controlled the distribution of the North China Sea, Qilian Sea, and Qinling Sea and also controlled the combination and separation of the three sea areas. At the same time, they controlled the variation of the sedimentary thickness of the Ordovician and the distribution of the sedimentary facies belt [32]. After the deposition of the Majiagou Formation, the Caledonian movement at the end of the Middle Ordovician uplifted the north China platform to land. The upper part of the Middle Ordovician Majiagou Formation in the basin underwent weathering and denudation for more than 130 million years, forming a set of reservoirs related to weathering crust. This set of reservoirs has experienced dolomitization and gypsum during the quasisyngenetic period, which laid the material basis for the reservoir. The selective dissolution during the epikarst period constructs the reservoir profile. Dissolution during burial and filling of various minerals determines the preservation of early dissolved pores and the final stage of reservoir. The Yanchang gas field is located in the southeast of Yishan slope (Figure 1), the proven reserves are more than 100 billion square, the reservoir is weathering crust type, and the main gas production interval is Majiagou Formation $M5_{1\text{-}2}$ submember. The Ordovician Majiagou Formation is composed of a set of epicontinental sea carbonate rocks and evaporites. According to the sedimentary cycle and lithologic association characteristics of M5 member, M5 member is divided from bottom to top into 10 submembers (Figure 2). The target interval of this study is $M5_{1\text{-}2}$ submember. The lithology is gypsum-bearing model pore argillaceous dolomite, algal-bonded dolomite, argillaceous dolomite, and a small amount of gypsum dolomite and tuffaceous mudstone. The reservoir quality is obviously controlled by sedimentary microfacies, karst landform, diagenesis, and small-scale structure.

3. Samples and Methods

164 samples (Figure 3) were collected from the $M5_{1\text{-}2}$ submember of the Lower Paleozoic Ordovician Majiagou Formation in the study area. The optical characteristics of minerals were observed under single polarizing microscope, orthogonal polarizing microscope, or convergent polarizing microscope to study the optical properties of minerals. The test instrument was 59XC-PC transreflective polarizing microscope.

Cathodic luminescence: 90 thin slices were detected and the samples were made into cathode luminescence thin slices. Put the sample into the sample room and open the vacuum system. Adjust the electron gun to the analytical position and start electron beam bombardment of the sample. CL8200 MK5 cathode luminescence device and OLYMPUS CX21 microscope were used in the experiment.

Fluid inclusion test: based on the principle that different concentrations of salt aqueous solutions have different freezing points, the freezing point Tm of the inclusion body fluid phase can be determined. According to the measured freezing point of the inclusion, the corresponding phase diagram can be used to calculate the liquid salinity of the inclusion. Zeiss polarization and fluorescence microscope, Linkam THM600 hot and cold table, and INVIA micro laser Raman spectrometer were used.

Carbon and oxygen isotope: start carbonate carbon dioxide online preparation device, set acidolysis reaction plate control temperature is 70°C–80°C. 0.2 mg–1 mg carbonate samples were put into the reaction bottle, the reaction bottle was sealed and put into the acidolysis reaction plate of the

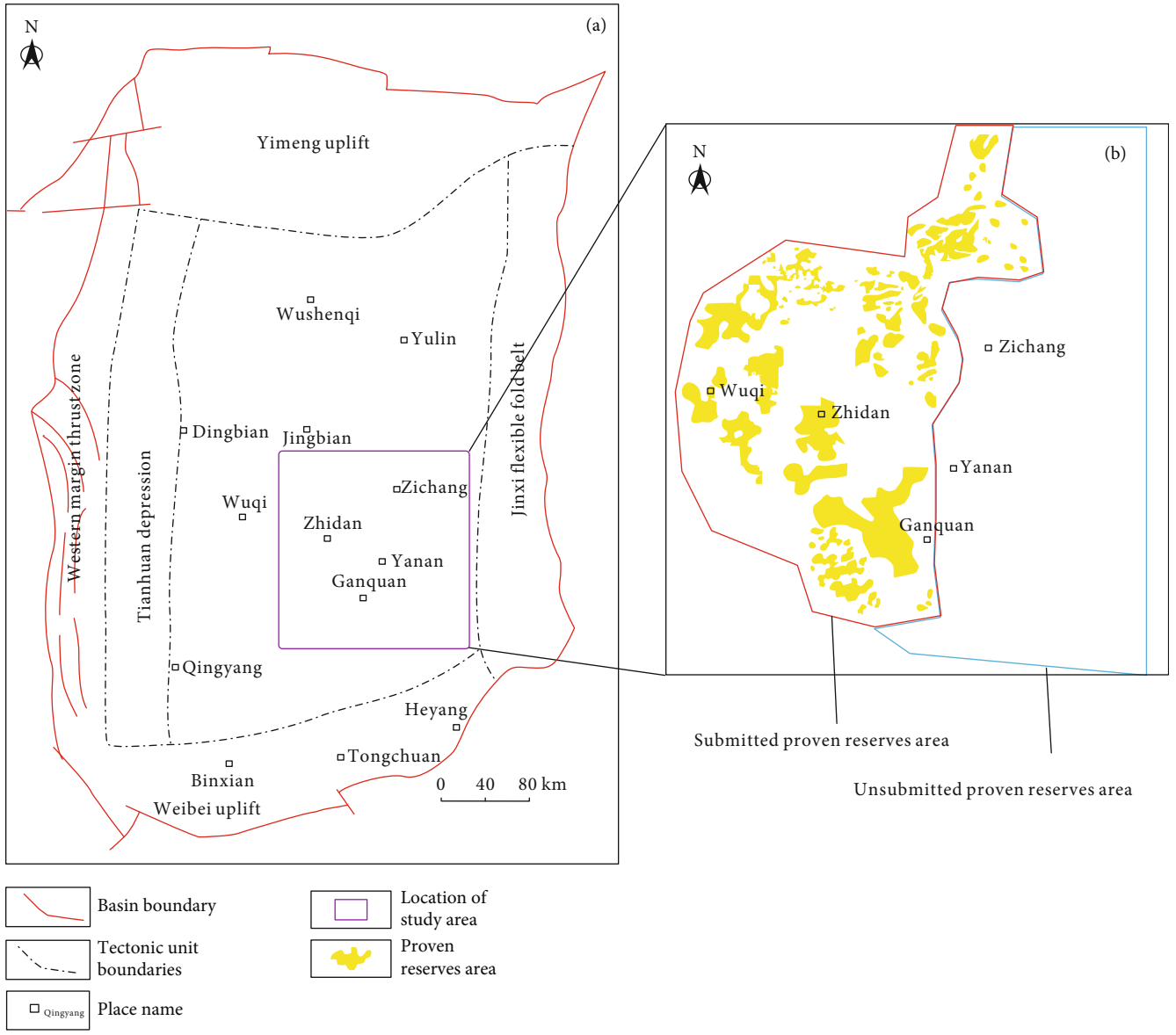

Figure 1: (a) Location of area in the Ordos Basin. (b) Reserve distribution area of the Yan'an gas field, yellow square shows the submitted proven reserves area.

preparation device, and the air in the reaction bottle was evacuated by helium. The phosphoric acid injection pump was started, and phosphoric acid was added. The reaction time was not less than 2 hours. The carbon dioxide of the acidolysis product was sent to the isotope mass spectrometer for detection. The stable isotope ratio mass spectrometer MAT 253 was used.

Sr isotope: carbonate rock powder by 0.5 mol/L dilute acetic acid bath ultrasonic three times, 10 minutes each. After centrifugation at 3300 rpm, the supernatant was evaporated to 1.5 mL 1.5 mol/L HCl. The solution was introduced by Cetac Aridus II membrane desolventizing system, and the $^{87}Sr/^{86}Sr$ isotope ratio was measured on Nu Plasma II MC-ICP-MS. During the determination, $^{86}Sr/^{88}Sr = 0.1194$ internal calibration instrument mass fraction and Sr isotope international standard material NIST SRM 987 were used as external standard calibration instrument drift.

4. Result

4.1. Lithology

4.1.1. The Lithology of Reservoir. The lithology of $M5_{1-2}$ submember of Majiagou Formation is anhydrite-bearing mud powder crystal dolomite, powder crystal dolomite, and karst breccia dolomite.

Anhydrite-bearing pore fine-powder crystal dolomite: gray, light gray gypsum spot dissolved pore fine-powder crystal dolomite (Figure 4(a)), the shape of the dissolved pores is mainly round and flat ellipse. Although the porous

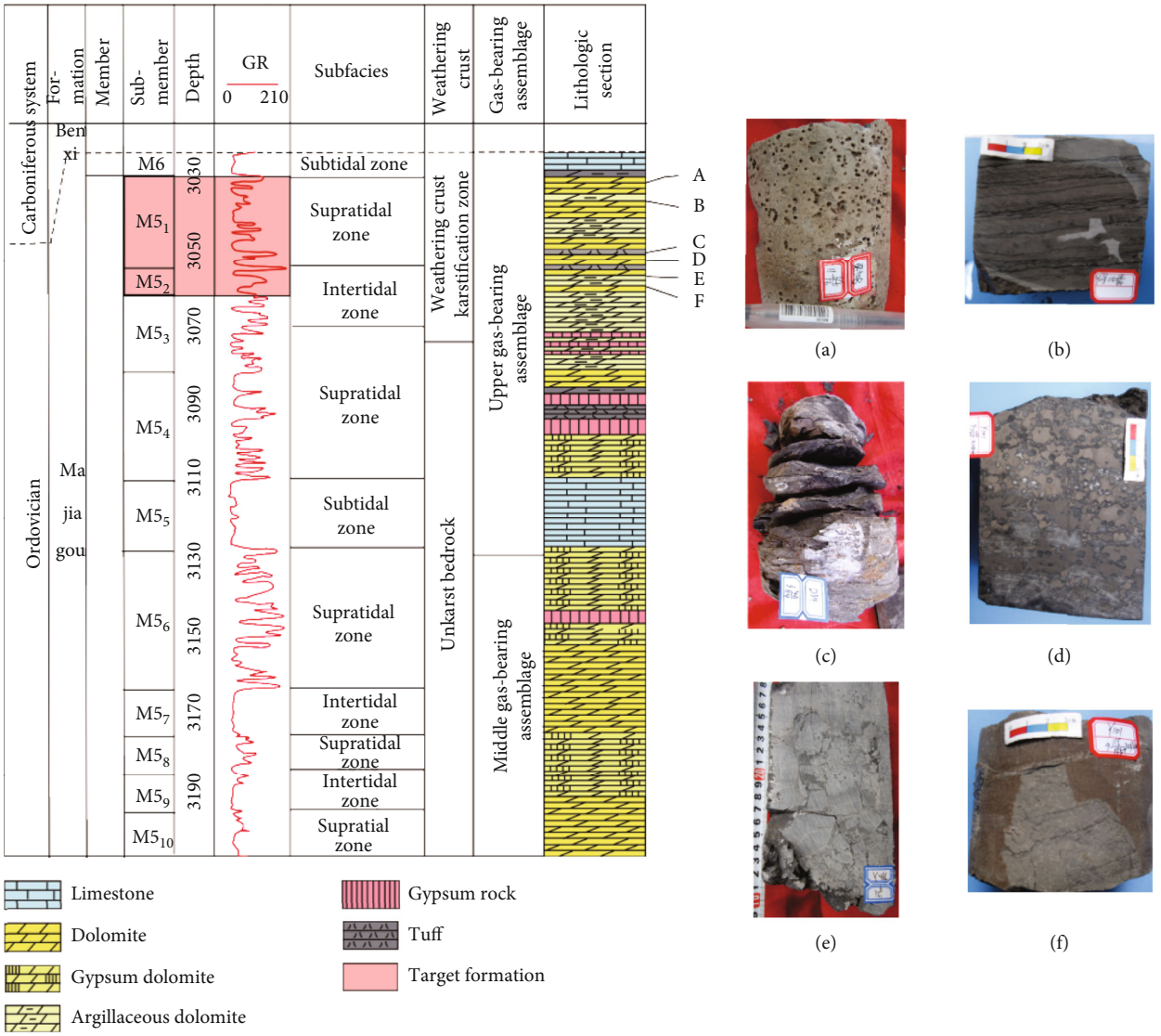

Figure 2: Stratigraphic and lithology histogram of the Yan'an gas field with photographs of the representative lithology of the gas field: (a) anhydrite-bearing mud powder crystal dolomite, (b) algal dolomite, (c) tuff, (d) fully filled anhydrite-bearing mud powder crystal dolomite, (e) karst breccia, and (f) fracture developed fine-powder crystal dolomite.

dolomite is filled by different materials at different times, the secondary pores are still relatively developed, which is a good reservoir space. The single-layer thickness of this kind of reservoir rock is generally 2–3 m, which is vertically interbedded with gray or light gray micrite powder crystal dolomite, mud-bearing dolomite, and karst breccia. In the study area, this kind of reservoir is distributed in $M5_1^1$, $M5_1^2$, $M5_1^3$, $M5_1^4$, and other layers, and the distribution of corrosion holes in the $M5_1^3$ layer is the most stable in the plane, which is also the main gas-producing layer in the study area.

Fine-powder crystal dolomite: mainly gray fine-powder crystal dolomite (Figure 4(b)). Dolomite is mostly inlaid with other-shaped crystals, with uniform lithology and massive structure. Dissolved pore is not developed, and fractures are developed. Therefore, the layer has high permeability storage capacity. The single layer thickness of reservoir is generally 1~2 m, which is mainly thin layer and widely distributed. This kind of reservoir rock is mainly distributed in $M5_2^2$ small layer, which developed horizontal and vertical fractures.

Karst breccia dolomite: in karst brecciated micrite powder dolomite, breccia is angular-subangular, no grinding circle, or has a certain degree of grinding circle (Figure 4(c)). Most of the breccia particle size is 1~10 cm, poor sorting. The breccia is argillaceous-powder crystalline dolomite, and the dissolution pores are not developed. A few breccias have gypsum dissolution pores, and the reservoir properties are generally poor. Gravel pores, fractures, or dissolved pores can be formed between breccias in some areas, which makes breccia dolomite become a better reservoir.

4.1.2. The Filling Substance. Crystalline mineral is the most direct evidence of fluid activity, recording the nature of fluid

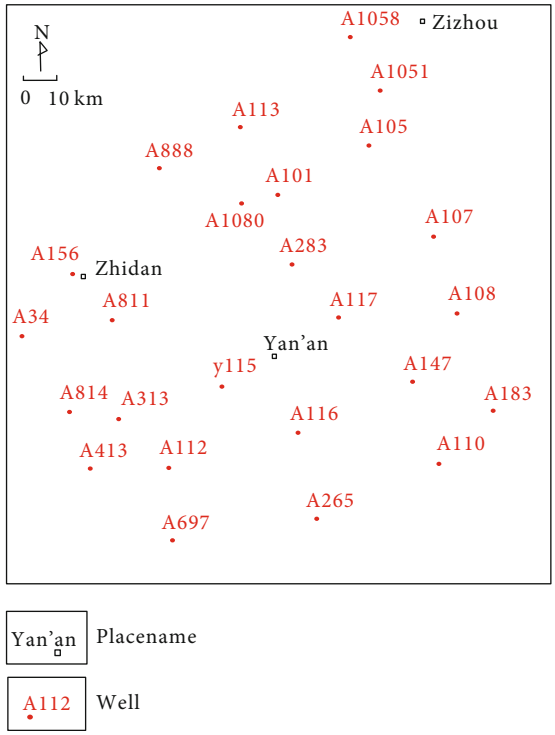

Figure 3: Location of the sampling well.

action and filling type. Through thin section analysis of samples in Yan'an area, there are mainly six typical crystalline minerals filled in dissolved pores and cracks.

Dolomite: as a filling material can be divided into three categories: seepage silt dolomite generally filled in the lower part of the pore, the formation time is earlier and formed in a relatively open system. The cleavage joints of late-filling saddle dolomite have slight bending and often show wavy extinction under orthogonal polarized light, mostly generated in the environment of high ground temperature. Iron dolomite is transformed from recrystallized dolomite under high temperature and hypoxia reduction environment into iron dolomite, which does not emit light under cathode ray (Figures 4(f)–4(j)).

Calcite: calcite filling is later than dolomite. Based on the core sample observations, calcite fillings can be divided into dark gray freshwater calcite and white bright crystal calcite. The formation of white bright crystal calcite is later than that of dark gray calcite, and the formation temperature is higher. The early calcite does not glow under the cathode ray, and the medium-term bright crystal calcite is mostly developed on the seepage silt dolomite. The dark red and bright orange red under the cathode ray are common ring structures. The late bright crystal calcite is formed in the residual space of dissolved pores, mostly developed in the late tectonic fractures, and does not emit light under the cathode ray (Figures 4(d), 4(e), and 4(j)).

Anhydrite: anhydrite is the main noncarbonate mineral in Lower Paleozoic. Anhydrite formed by metasomatism at low temperature generally has plate-like, needle-like, and cluster-like crystals and does not emit light under cathode luminescence (Figure 4(k)).

Quartz: quartz cementation has two stages. Quartz crystals formed in the early stage have relatively good self-forming degree and are relatively clean and bright. Quartz formed in the late stage has a small number and poor crystal shape. Quartz crystals often contain more impurities and inclusions, which are formed after kaolinite cement and have great damage to reservoir pores (Figure 4(g)).

Fluorite: fluorite contains a small amount of rare earth elements, which is occasionally seen in the Lower Paleozoic carbonate rocks. Fluorite is colorless or light yellow, light green, etc. The interspersed double crystals are observed. Negative high protrusion under single polarizing mirror; cathodic radiation is blue (Figure 4(i)).

Clay minerals: kaolinite is the main component of terrigenous clastic clay minerals in Lower Paleozoic carbonate rocks. It is white and belongs to monoclinic or triclinic system. The grain size is small and hexagonal plate, and the aggregate is flake or soil. Cathodic radiation emits dark blue and indigo light, which reduce reservoir porosity (Figure 4(j)).

4.2. Geochemistry

4.2.1. Carbon and Oxygen Isotopes. The experimental data show that the $\delta^{18}O$ of bulk rock carbonates range from −11.36‰ to −6.54‰ VPDB, with an average of −8.58‰ VPDB; $\delta^{13}C$ ranged from −6.30‰ to 1.01‰ VPDB, with an average of −1.15‰ VPDB (Table 1). The distribution range of $\delta^{18}O$ and $\delta^{13}C$ is within the distribution range of $\delta^{18}O$ and $\delta^{13}C$ of all carbonate components sampled by laser microscopy. The $\delta^{18}O$ of micrite dolomite ranged from −10.50‰ to −1.12‰ VPDB, with an average of −5.04‰ VPDB. The $\delta^{13}C$ range from 4.33‰ to 4.26‰ VPDB, with an average of 1.86‰ (Table 1). The $\delta^{18}O$ of dolomite filled in dissolution pores and fractures ranged from −11.90‰ to −2.05‰ VPDB, with an average of −7.08‰ VPDB; $\delta^{13}C$ ranged from −6.03‰ to 1.05‰ VPDB, with an average of 0.34‰ VPDB (Table 1). The $\delta^{18}O$ of calcite filled in dissolution pores and fractures ranged from −17.08‰ to −3.89‰ VPDB, with an average of 11.84‰ VPDB. $\delta^{13}C$ ranged from −11.06‰ to −2.67‰ VPDB, with an average of 1.95‰ VPDB (Table 1). In general, the $\delta^{18}O$ and $\delta^{13}C$ of filled dolomite are lower than those of micrite dolomite. The reason is that the formation of filled dolomite is late affected by freshwater leaching, burial, and organic matter. The $\delta^{18}O$ and $\delta^{13}C$ of dolomite and calcite filled in pores are lower than micritic dolomite because the cements precipitate under high-temperature burial conditions and are related to freshwater. The change of $\delta^{13}C$ of micritic carbonate mainly occurs in the early diagenesis stage, and the sediments are not consolidated. When the temperature or isotopic composition of diagenetic pore water is very different from that of surrounding seawater, it generally does not occur in the burial stage. The $\delta^{18}O$ and $\delta^{13}C$ of carbonates formed by karstification in dissolution pores, caves, and fractures mainly depend on the composition and temperature of pore water. The $\delta^{18}O$ and $\delta^{13}C$ of calcite cements are lower than those dolomite cements.

(a) (b)

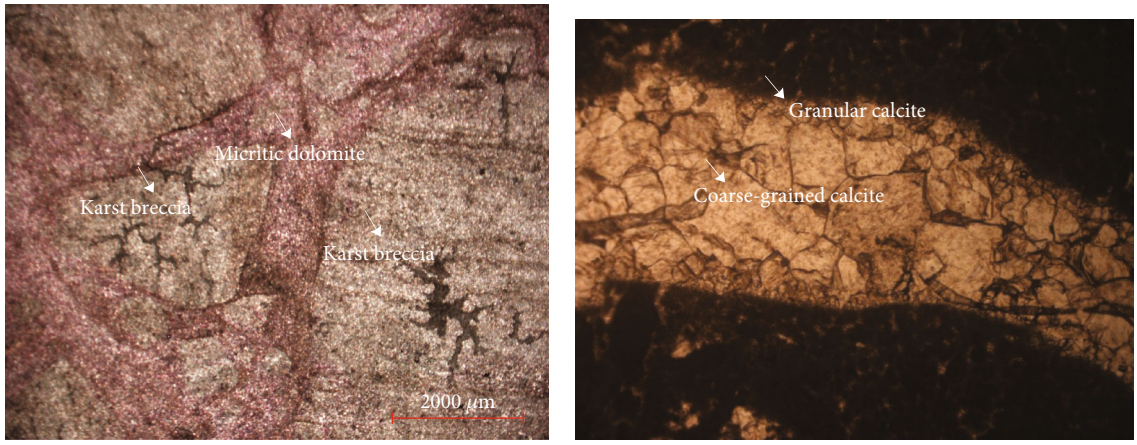

(c) (d)

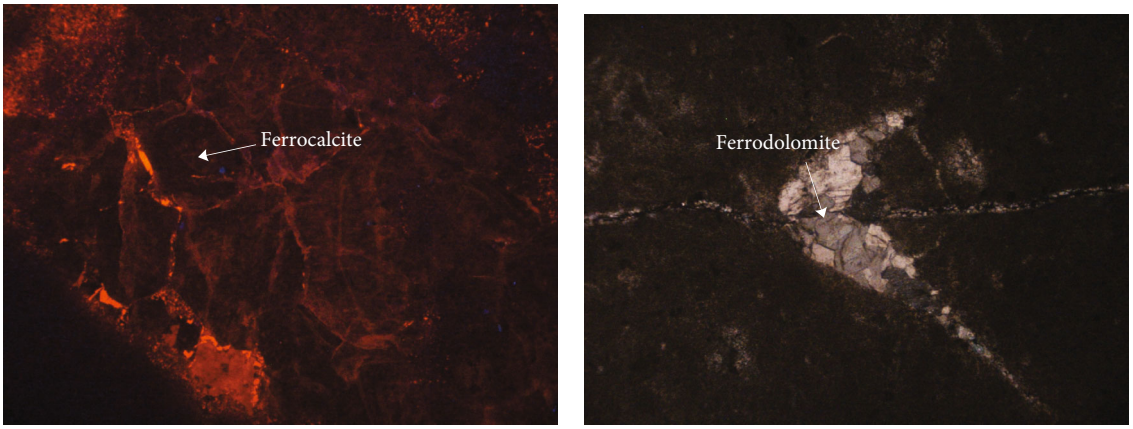

(e) (f)

Figure 4: Continued.

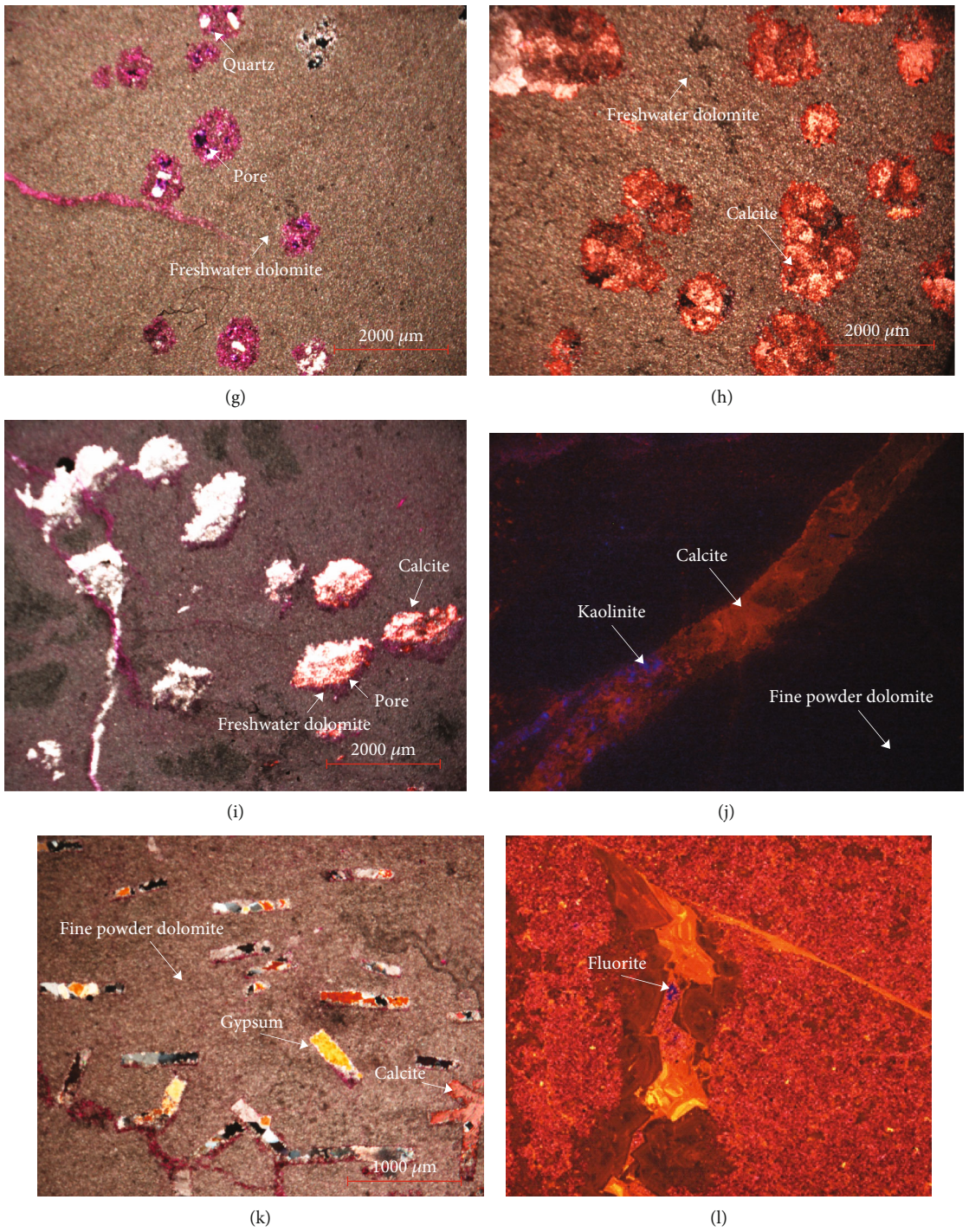

Figure 4: Photos of reservoir rock types and fillings in $M5_{1-2}$ submember of Majiagou Formation. (a) Crystal dolomite, moldic pores in anhydrite accretions. (b) Fine-powder dolomite, fracture development. (c) Karst breccia dolomite, dissolution pores between breccias. (d) Photomicrograph showing fractures filled with granular calcite and coarse-grained calcite. (e) Optical CL photomicrograph of ferrocalcite is filled in the fracture. (f) Optical CL photomicrograph of ferrodolomite is filled in moldic pores. (g) Plane light optical photomicrograph of moldic pores in anhydrite accretions, completely filled with freshwater dolomite. (h) Plane light optical photomicrograph of moldic pores in anhydrite accretions, completely filled with calcite. (i) Plane light optical photomicrograph of the fracture is filled with saddle dolomite. (j) Optical CL photomicrograph of the fracture is filled with calcite and kaolinite. (k) Plane light optical photomicrograph of gypsum crystals, filling calcite in tabular moldic pores in gypsum. (l) Optical CL photomicrograph of fluorite is filled in the pores.

Table 1: Summary of $\delta^{18}O$ and $\delta^{13}C$ values for different types of carbonate of Ordovician in Yan'an area.

Rock type	Sample numbers	$\delta^{13}C$ (‰)		$\delta^{18}O$ (‰)	
		Range	Average	Range	Average
Bulk rock	59	−6.30‰ to 1.01‰	−1.15‰	−11.36‰ to −6.54‰	−8.58‰
Mud powder crystalline dolomite	22	−4.33‰ to 4.26‰	1.86‰	−10.50‰ to −1.12‰	−5.98‰
Dissolution pores filled with dolomite	6	−6.30‰ to 1.05‰	0.34‰	−11.90‰ to −2.05‰	−7.08‰
Dissolution pores filled with calcite	7	−11.06‰ to −2.67‰	−1.95‰	−17.08‰ to −3.89‰	−11.84‰

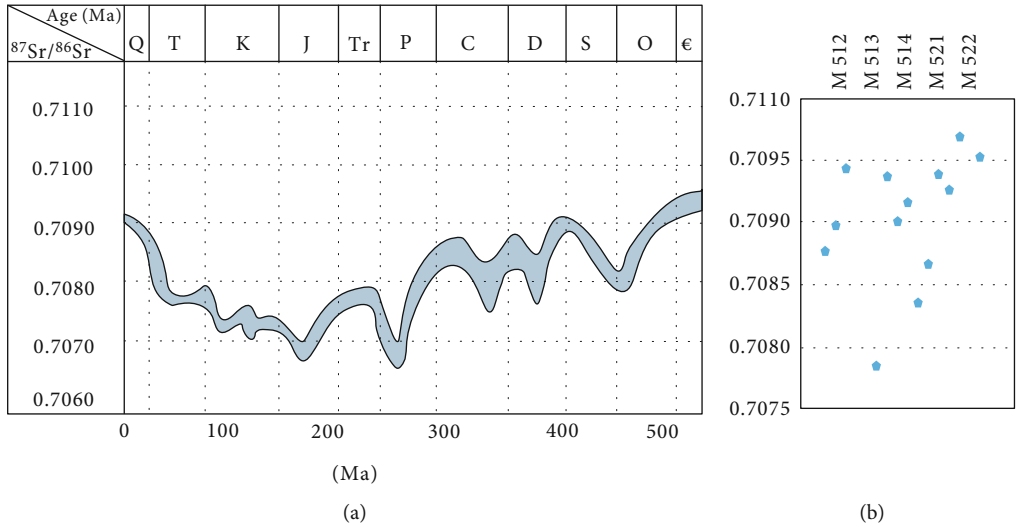

Figure 5: $^{87}Sr/^{86}Sr$ distribution of strontium isotope. (a) Global Quaternary Cambrian strontium isotopic evolution curve. (b) Strontium isotope $^{87}Sr/^{86}Sr$ distribution in $M5_{1\text{-}2}$ submember of Majiagou Formation of Middle Ordovician in Yan'an area.

4.2.2. Strontium Isotopes. According to the latest international geological chronology published in 2020, the top boundary of the Middle Ordovician Majiagou Formation is 458.4 Ma, and the corresponding $^{87}Sr/^{86}Sr$ ratios are 0.7077–0.7081 (Figure 5(a)). The evolution trend of strontium isotope in the study area is also shown as the monotonous increase of $^{87}Sr/^{86}Sr$ ratio over time. The $^{87}Sr/^{86}Sr$ ratio of $M5_{1\text{-}2}$ submember of Majiagou Formation host rocks ranges from 0.7076 to 0.7098, 0.70952 to 0.70958 for $M5_2{}^2$, 0.70925 to 0.70968 for $M5_2{}^1$, 0.70835 to 0.70937 for $M5_1{}^4$, 0.70784 to 0.70936 for $M5_1{}^3$, and 0.70876 to 0.70942 for $M5_1{}^2$ (Figure 5(b)).

The strontium isotope test results show that the $^{87}Sr/^{86}Sr$ ratio of the acid salt rocks in the upper member of the Middle Ordovician Majiagou Formation is between 0.7078 and 0.7118. The test data is higher than the standard value, indicating that after the Ordovician deposition, the Ordos Basin was uplifted as a whole, and the dissolved silicates of atmospheric freshwater provided shell source strontium to the marine carbonate, resulting in an increase of $^{87}Sr/^{86}Sr$ ratio.

4.2.3. Fluid Inclusion. Inclusions of calcite filled in fractures and dissolved pores in the $M5_{1\text{-}2}$ submember reservoir are selected. Single liquid brine inclusions are colorless and transparent, mostly elliptical and strip-shaped, mostly 3–5 μm in size, and the boundary of inclusions is fuzzy. Gas-liquid two-phase brine inclusion: the inclusion is clear and transparent, the boundary is clear, mostly oval, a small number of irregular shape, most size 4 to 5 μm, and gas-liquid ratio is about 4% to 6%. Gaseous hydrocarbon inclusions are mainly composed of single-phase gaseous hydrocarbons. Under transmission light, they are generally gray-black and have high bulges. Larger individual gaseous hydrocarbon inclusions are elliptical, irregular, or negative crystalline and are randomly distributed in calcite or fluorite cleavages or fractures filled in reservoir pores, caves, and fractures.

Microscopic temperature measurement of gas-liquid two-phase brine inclusions and hydrocarbon inclusions in calcite in fractures and dissolved pores was carried out. The main body of the homogenization temperature measured by the two types of calcite is 79.5 to 193°C (Figure 6), and the inclusions in the calcite are filled in the holes. The main body of the homogenization temperature measured is 90 to 180°C, which can be divided into two phases. The first phase is mainly 90 to 120°C, and the main peak is 100 to 110°C. The second phase is mainly 120 to 170°C, and the main peak is 160 to 170°C. For calcite filled in cracks, the measured main body of homogenization temperature is 80 to 180°C. The first phase is mainly 80 to 140°C (Figure 6), and the main peak is 120 to 130°C. The second phase is mainly 140 to 180°C, and the main peak is 150 to 160°C (Table 2).

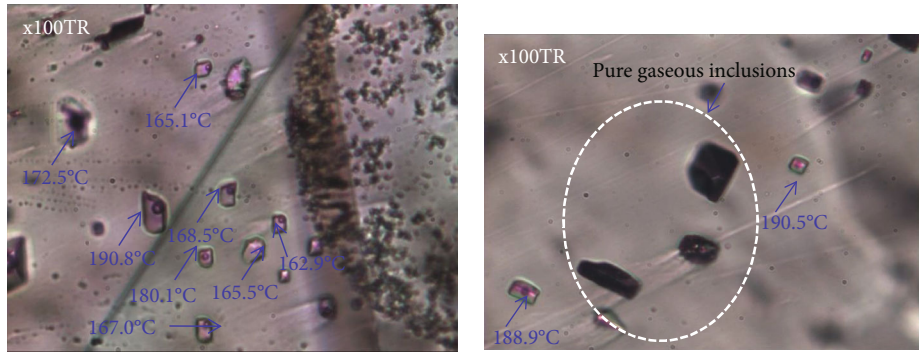

(a) (b)

Figure 6: Photomicrographs of fluid inclusion. (a) Large number of brine inclusions developed in calcite filled with dissolved pores. (b) Salt water inclusions and pure gas inclusions developed in calcite filled with dissolved pores.

Table 2: Fluid inclusion characteristics of $M5_{1\text{-}2}$ submember of Middle Ordovician Majiagou Formation in Yan'an area.

Well	Feature	Formation	Depth (m)	Size (μm)	Gas-liquid ratio (%)	Homogenization temperature (°C)	Salinity (wt.% eq. NaCl)
A1510	Fracture-filling calcite	$M5_1^2$	2841.75	5 to 20	4 to 15	129.4 to 156.4	11.1 to 18.9
A697	Fracture-filling calcite	$M5_1^{1\text{-}2}$	3226.26	6 to 20	1 to 10	93.6 to 149.3	13.7 to 21.7
A147	Fracture-filling calcite	$M5_1^{2\text{-}4}$	2583.80	2 to 8	3 to 5	86 to 136.5	4.6 to 16.3
A156	Fracture-filling calcite	$M5_1^2$	3619.25	4 to 18	3 to 5	112 to 218.4	7.3 to 17.9
A1508	Dissolution pores filled with calcite	$M5_2$	2754.68	5 to 10	2 to 10	91.1 to 123.7	15.2 to 21.5
A117	Dissolution pores filled with calcite	$M5_1^{3\text{-}4}$	2749.67	3 to 12	5 to 8	112 to 179.3	6.4 to 10.38
A110	Dissolution pores filled with calcite	$M5_1^{1\text{-}3}$	2531.60	2 to 10	3 to 8	94 to 169.5	5.3 to 15.4
A108	Dissolution pores filled with calcite	$M5_1^{1\text{-}3}$	2456.50	2 to 15	5 to 8	102.1 to 135.4	7.8 to 16.7
A103	Dissolution pores filled with calcite	$M5_1^4$	3047.70	2 to 17	5 to 8	98 to 143.7	10.3 to 16.4
A413	Dissolution pores filled with calcite	$M5_1^2$	3533.28	4 to 13	4 to 6	96 to 152.9	9.5 to 20.7
A265	Dissolution pores filled with calcite	$M5_1^4$	2898.05	3 to 16	4 to 6	90 to 133.4	10.4 to 21.5

According to the diagram of the relationship between the homogenization temperature and salinity of the inclusions in the study area, it can be concluded that the homogenization temperature and salinity of the inclusions in the study area are divided into five intervals: the homogenization temperature is 70 to 100°C, and the salinity is 0 to 3.5% (Figure 7). Such inclusions may be buried in a certain depth, and the atmospheric freshwater enters the strata through fracture or interlayer interface. The homogenization temperature is 70 to 100°C, and salinity is more than 3.5%. Such inclusions can be formed when the strata are buried in a certain depth range according to the normal geothermal gradient without the influence of atmospheric freshwater. The homogenization temperature is 100 to 160°C, and salinity is 0 to 3.5%, which belongs to the normal buried depth temperature. However, the low salinity may be due to the surface exposure of the formation when the structure is uplifted, which is affected by the atmospheric freshwater, resulting in the decrease of the salinity of the formation water. It may also be related to the fracture, and the atmospheric freshwater enters the formation along the fracture. The homogenization temperature is 100 to 160°C, and the salinity is more than 3.5%. When the stratum is deposited, it does not directly contact with atmospheric freshwater, and the stratum is in a closed environment. When the burial depth reaches a certain degree, the holes are filled and the inclusions are captured. The average temperature is 160 to 200°C, and the salinity is >3.5%. The formation environment is when the rock layer is buried to a certain depth without the influence of atmospheric freshwater, but the formation

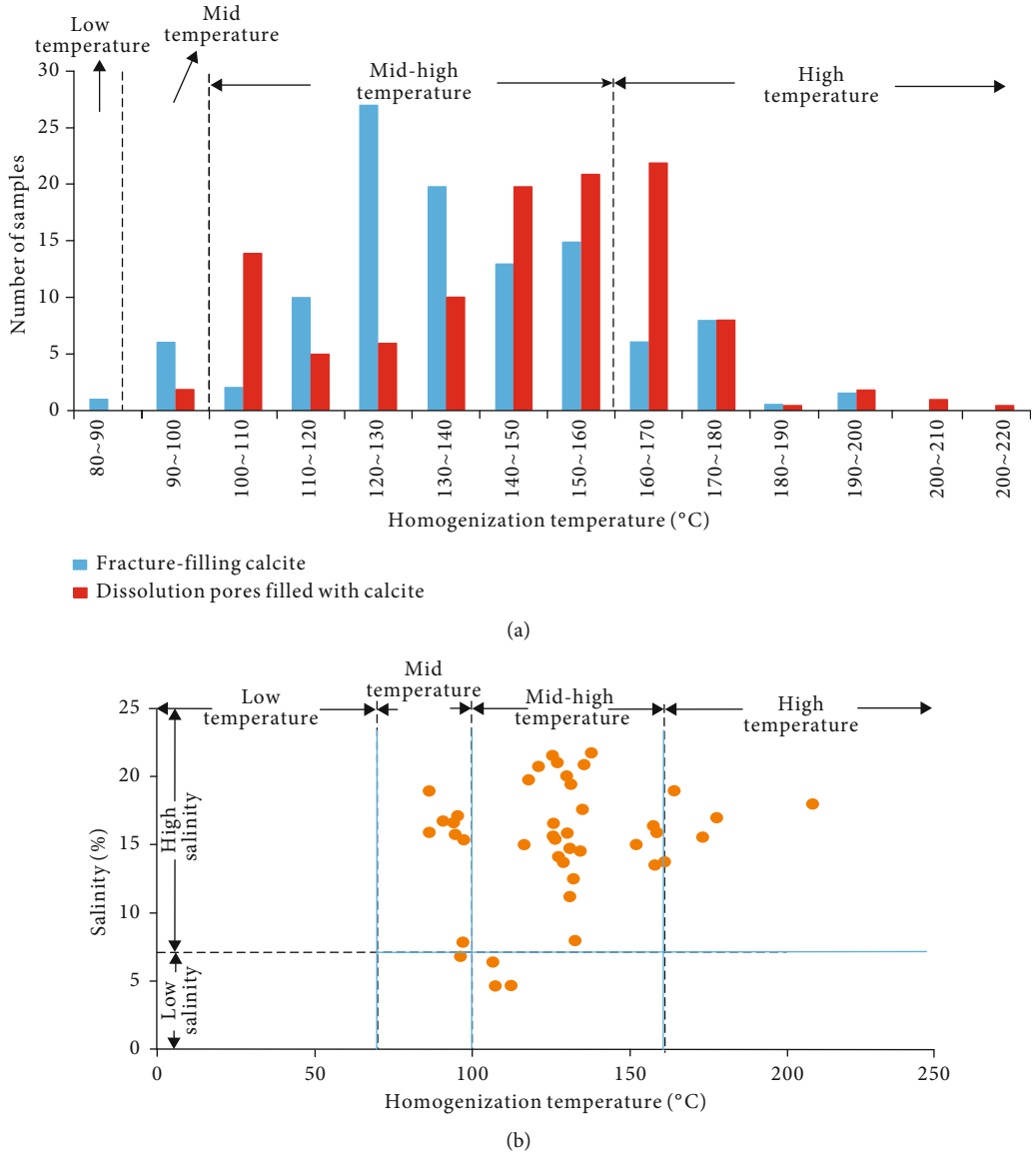

FIGURE 7: (a) The distribution map of homogenization temperature. (b) The relationship between homogenization temperature and salinity in $M5_{1-2}$ submember of Middle Ordovician Majiagou Formation in Yan'an gas field.

is affected by the hot water, forming the inclusions with high temperature and high salinity. The salinity value is affected by the hydrothermal solution and slightly decreases.

5. Discussion

5.1. Diagenetic Environments

5.1.1. Marine Diagenetic Environments. The evaporation platform and limited platform are characterized by salted seawater, which is called evaporation seawater diagenetic environment. With the strong evaporation of seawater in the hot and arid climate, carbonate and evaporated salt in the salinized lagoon accumulated and precipitated one after another, forming a sediment interbedded with mechanical deposition and chemical precipitation. Calcium carbonate formed quasicontemporaneous dolomite under the metasomatism of salinized brine, and the ash mud in the supratidal and intertidal zones also formed quasicontemporaneous dolomite under the action of capillary concentrated dolomitization. Then, the remaining salinized brine flows downward, making the lower sediments reflux and penetrate dolomitization, forming reflux and penetrate dolomite.

Quasicontemporaneous dolomite is formed in the environment of high Mg^{2+} ion concentration, the metasomatism and crystal growth rate are too fast, the crystal form is fine and heterogeneous, and the crystal order is low. The X-ray diffraction analysis data showed that the order degree of paracontemporaneous dolomite was 0.45–0.75, with an average of 0.63. Evaporative evaporation platform and limited platform are anoxic reduction environment. Compared with freshwater dolomite cements, the quasicontemporaneous argillaceous dolomite formed in this environment is characterized by high carbon and oxygen isotopes.

5.1.2. Meteoric Freshwater Diagenetic Environments. Atmospheric freshwater diagenetic environment is formed during the decline of sea level so that carbonate strata are completely exposed to atmospheric freshwater environment. According to the time when the strata are exposed to the surface, the atmospheric freshwater diagenetic environment can be divided into quasisimultaneous atmospheric freshwater environment and supergene atmospheric freshwater diagenetic environment.

The main diagenesis of the atmospheric freshwater diagenetic environment in the quasicontemporaneous period of the evaporation platform is dissolution and cementation. The atmospheric freshwater diagenetic environment is divided into seepage zones above the phreatic surface, phreatic zones below the phreatic surface, and mixed water zones below the phreatic surface. Under the lowest sea level, the gypsum salt dissolution collapse breccia, calcareous dolomite, quasisyngenetic dolomite, and lower mixed water dolomite are formed. The main role of the atmospheric freshwater diagenetic environment in the open sea platform and the platform margin during the quasisyngenetic period is cementation and quasisyngenetic dolomitization, and the beach dolomite, dolomitic granular limestone, and open sea platform limestone are below the sea level.

The atmospheric freshwater diagenetic environment in the supergene period is divided into vadose zone, horizontal underflow zone, and deep detention zone from the phreatic surface (Figure 8). The main diagenesis of the vadose zone are dissolution and cementation, as well as dedolomitization and degypsumization. In the case of fracture development, dissolution forms a series of longitudinally distributed dissolution ditches, and the water movement mode is vertical pipe flow, which is carried out in the way of downward diffusion when the fracture is not developed. The vicinity of the phreatic surface is a phreatic zone, and the water body mainly flowed in the horizontal direction. The main diagenesis is cementation. The deep detention zone is below the horizontal underflow zone, and the main diagenesis is mixed water dolomitization.

5.1.3. Burial Diagenetic Environments. Ordos Basin experienced the processes of early deposition, middle uplift exposure, and late burial. Buried dolomite was formed in the deep burial stage and had sufficient crystallization time. Its dolomite had high degree of order, which was between 0.82 and 1.0. However, hydrothermal dolomite had rapid dolomitization and low degree of order, which was between 0.52 and 0.77. Due to the high temperature in the burial diagenetic environment, the cement has the characteristics of low-carbon oxygen isotope, which is different from the isotope characteristics of the reduction environment in the atmospheric freshwater subsurface zone. Therefore, although it does not emit light under the irradiation of cathode ray, it can be distinguished by its low carbon and oxygen isotope.

5.2. Diagenesis Evolution. The primary pores of carbonate rocks are mainly intergranular pores of micritic limestone or quasicontemporaneous dolomite, and the original porosity is generally 70%. In the syngenetic stage, the early cementation and quasicontemporaneous dolomitization greatly reduce the original porosity.

In the early diagenesis stage, the carbonate strata of $M5_{1\text{-}2}$ experienced the interaction of early cementation and freshwater leaching in the process of continuous burial and intermittent exposure with the rise and fall of the sea level in the early Paleozoic. In the process of continuous burial, compaction and pressure solution further reduced the original porosity. At this stage, the maximum burial depth within the carbonate platform was 2000 m on average. Early cementation caused the loss of most of the original porosity, and the porosity decreased to less than 10%. During the intermittent exposure of the carbonate platform evaporation tidal flat stratum, the soluble mineral gypsum and stone salt in the atmospheric freshwater seepage zone and the atmospheric freshwater subsurface flow zone are dissolved, and the seepage sand is filled. A large number of corrosion holes are formed in the upper part of the seepage zone. Most of the corrosion holes in the lower part of the seepage zone and the subsurface flow zone are filled by the seepage sand, and the pores are filled by calcite. In addition, the gypsum salt layer due to the dissolution of the formation caused by dissolution collapses to form dissolution breccia and formed a large number of dissolution pores. At the same time, the residual brine in the evaporation platform and the limited sea platform is refluxed and penetrated so that the quasicontemporaneous dolomite is stabilized and further recrystallized, and the limestone is refluxed and penetrated into dolomitization, forming a powder and fine-powder dolomite reservoir with a large number of intergranular pores.

The late Caledonian movement completely uplifted the whole Ordos Basin, and the exposed surface of the Lower Paleozoic carbonate rocks was eroded, forming a large-scale paleokarst landform. At the same time, with the development of paleokarst landform in the basin, the upper atmospheric freshwater seepage zone and the lower atmospheric freshwater subsurface flow zone were formed at the top of the Ordovician Majiagou Formation, and the widely distributed paleokarst reservoirs were developed. The dissolved pores were widely developed, and a large range of degypsumization and dedolomitization occurred.

In the middle of Hercynian movement, a large-scale transgression occurred in Ordos Basin, which made the Lower Paleozoic carbonate strata enter the burial stage again. By the end of Permian, it entered the deep burial stage. The burial depth at the top of Ordovician reached 1700 m again, and by the end of Triassic, it reached 3000 m quickly. The whole Lower Paleozoic strata entered the deep burial stage. The carbonate strata of $M5_{1\text{-}2}$ entered the deep burial stage, and the buried organic matter entered the mature stage. The formation water containing a large number of organic acids entered the Lower Paleozoic carbonate strata along faults and fractures, causing a large range of dissolution in the burial stage. A series of diagenetic traps with composite reservoir space were formed along the weak structural areas. The faults and fractures formed during the tectonic movement provide a channel for the upward migration of underground hydrothermal fluid. The intrusion of underground hydrothermal fluid causes hydrothermal

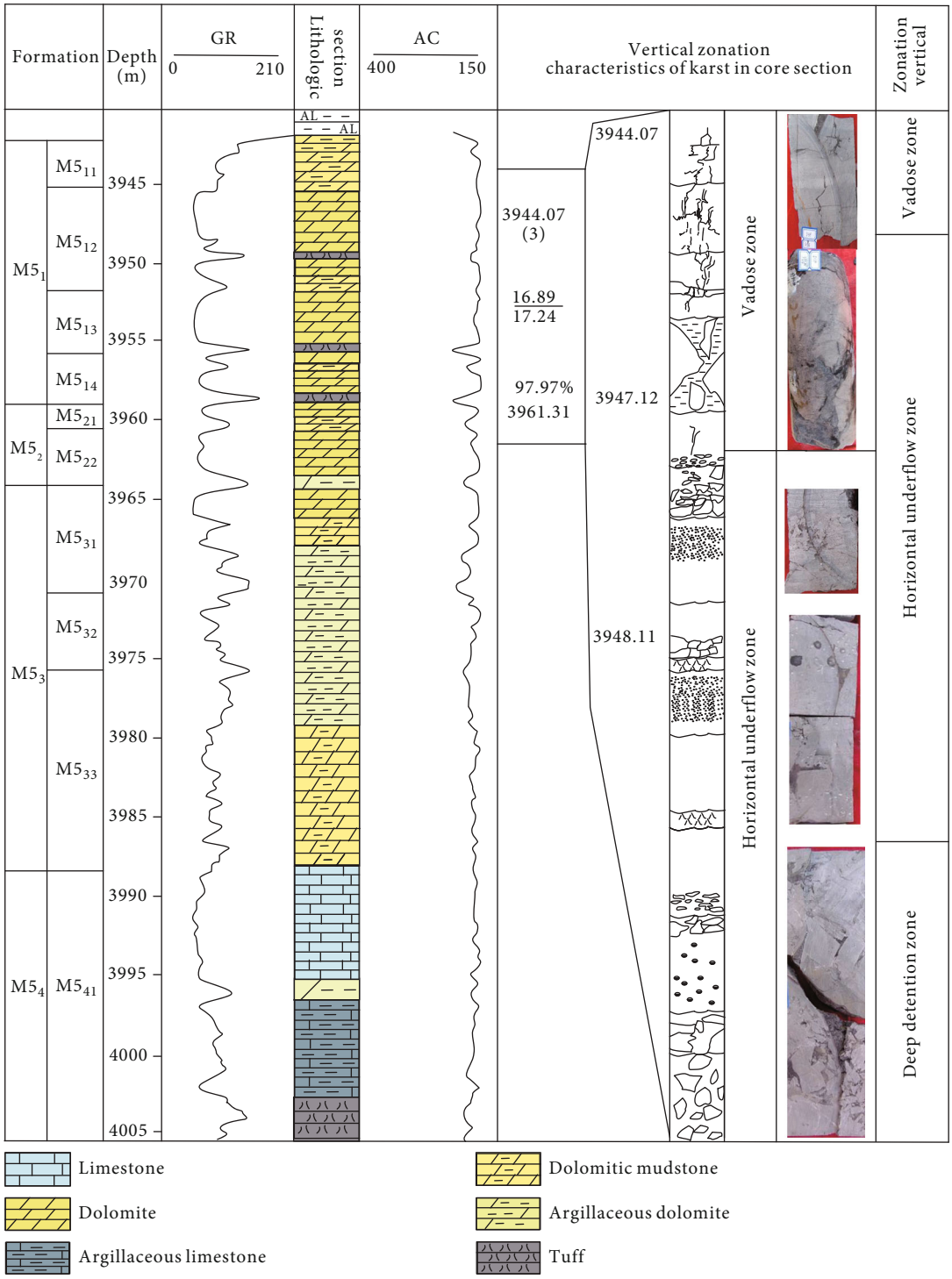

Figure 8: Vertical zonation diagram of ancient karst of well A34.

dolomitization of limestone strata around the fault zone to form hydrothermal dolomite distributed along the fault zone.

Dolomitization and dissolution are important constructive factors of reservoir formation; compaction, cementation, and dolomite removal are the main destructive factors for reservoir. The dissolution occurred in the sedimentary period, the early burial diagenesis, and the land exposure period, and the land exposure period was the strongest. Dolomitization mainly occurs in the postdepositional quasi-syngenetic period, the early diagenetic stage of shallow burial, the mixed water zone in the supergene period, and the development period of tectonic fractures. The compaction mainly occurs before the sediment has not been consolidated, and the pressure solution is the continuation of the compaction. Dedolomite mainly occurs in the surface conditions, and cementation occurs from the beginning to the end

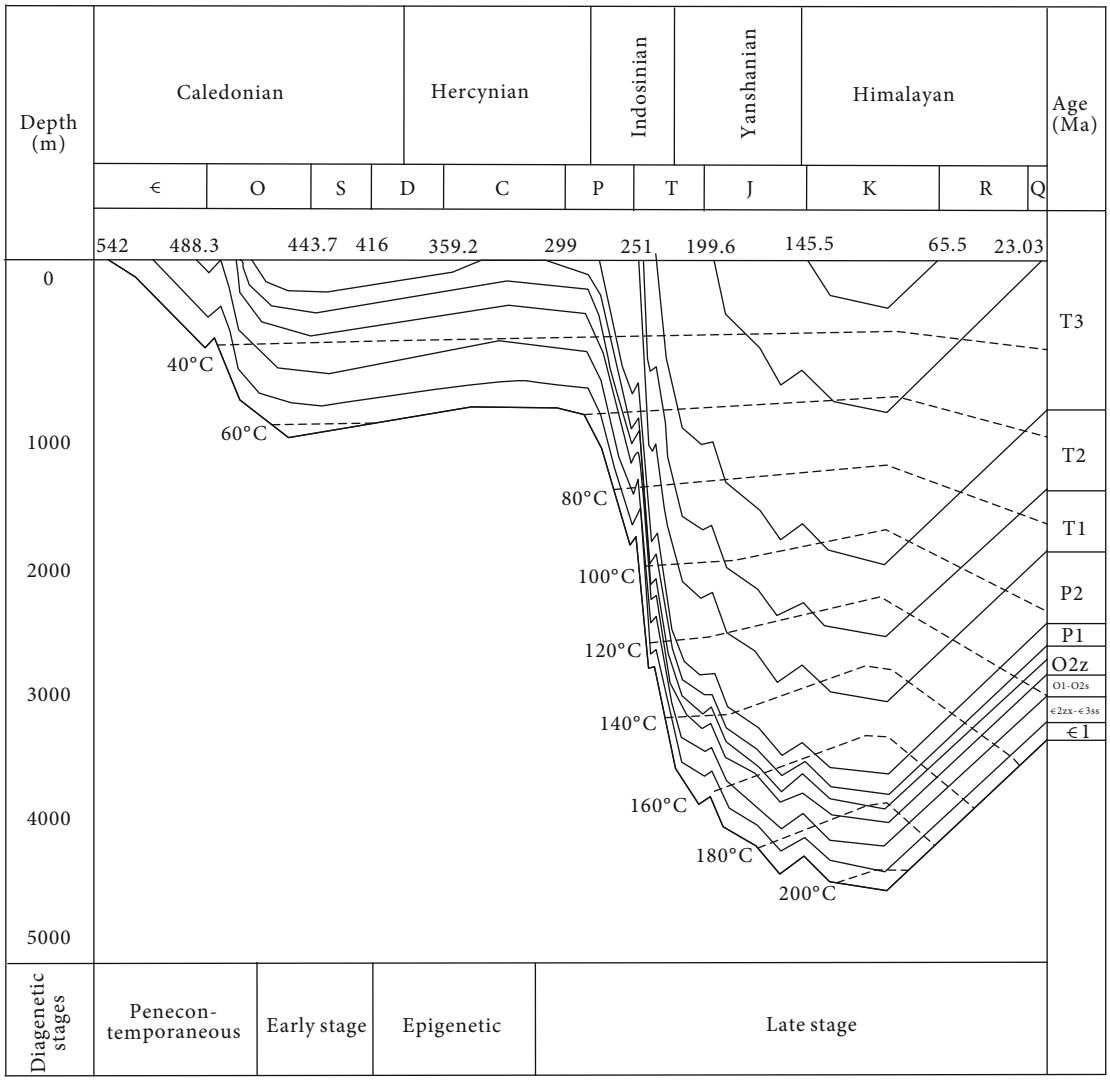

Figure 9: Reservoir burial history—diagenesis history of $M5_{1-2}$ submember of Ordovician Majiagou Formation in the study area.

of diagenesis. The pore water that dissolves the carbonate takes the carbonate to precipitate elsewhere (Figure 9).

6. Conclusions

The $M5_{1-2}$ reservoir in Yan'an gas field is mainly composed of gypsum-mud powder crystalline dolomite, mud powder crystalline dolomite, and breccia dolomite. The reservoir has thin layer and large area distribution. The pore types are mainly gypsum mold pores, intergranular (dissolved) pores, intragranular dissolved pores, and micro fractures, which often occur in composite types. Common fractures are gypsum mold pores; fractures are intergranular (dissolved) pore combination. The reservoir has strong macroscopic and microscopic heterogeneity. The pore filling minerals are mainly dolomite and calcite and a small amount of quartz, gypsum, and kaolinite. The filling degree has obvious zonation.

The $\delta^{18}O$ and $\delta^{13}C$ values of carbonate cements in fractures and dissolution cavities are significantly negative, and the $^{87}Sr/^{86}Sr$ ratio is higher than the standard value which indicates the atmospheric freshwater activity; high-temperature minerals and inclusions higher than 200°C prove the existence of local hydrothermal solution.

The sedimentary period of the $M5_{1-2}$ submember of the Majiagou Formation in Yan'an area is dominated by weakly oxidized seawater environment. The diagenesis experienced the evolution process of (quasi)contemporaneous-early diagenetic mixed water environment ⟶ calcite cementation ⟶ dissolution in supergene atmospheric freshwater environment ⟶ calcite cementation, metasomatism, and acid fluid dissolution in middle-late diagenetic formation water environment. The sedimentary diagenesis process is the product of multiple fluids, and the fluid sources include seawater, atmospheric freshwater, hydrocarbon fluid, and deep (thermal) fluid.

Data Availability

The data used to support the findings of this study are available from the corresponding authors upon request.

Conflicts of Interest

Author Haiyan Wu was employed by the Research Institute of Yanchang Petroleum (Group) Co., Ltd., Xi'an, China. The remaining authors declare that the research was conducted in the absence of any commercial or financial relationships that could be construed as a potential conflict of interest.

Authors' Contributions

YW was responsible for writing—original draft preparation. All authors contributed data and analysis tools. All authors have read and agreed to the published version of the manuscript.

Acknowledgments

We greatly thank Chao Gao and Yanjun Wu for providing the valuable information. The study is supported by the China Geological Survey Project: "China Journal of Mineral Geology" (No. DD20190379-53) and the China Geological Survey's Comprehensive Integration and Service of Mineral Geology and Metallogenic Law in China (No. DD20160346).

References

[1] V. Baqués, E. Ukar, S. E. Laubach, S. R. Forstner, and A. Fall, "Fracture, dissolution, and cementation events in Ordovician carbonate reservoirs, Tarim Basin, NW China," *Geofluids*, vol. 2020, Article ID 9037429, 28 pages, 2020.

[2] H. J. Yang, J. F. Han, C. H. Sun, F. H. Wang, and Y. Zheng, "Supersonic swirling characteristics of natural gas in convergent-divergent nozzles," *Acta Petrolei Sinica*, vol. 8, no. 1, pp. 114–119, 2011.

[3] D. Xiao, X. C. Tan, A. H. Xi, H. Liu, S. J. Shan, and J. W. Xia, "Palaeokarst characteristics of carbonate rocks of the Middle Permian Maokou Formation in southern Sichuan Basin: Example of strata-bound eogenetic karst in palaeo-continental settings," *Journal of Palaeogeography*, vol. 17, no. 4, pp. 457–476, 2014.

[4] H. G. Machel, "Investigations of burial diagenesis in carbonate hydrocarbon reservoir rocks," *Journal of the GeologicalAssociation of Canada*, vol. 70, no. 3, pp. 398–420, 2005.

[5] X. H. Ma, Y. Yang, L. Wen, and B. Luo, "Distribution and exploration direction of medium- and large-sized marine carbonate gas fields in Sichuan Basin, SW China," *Petroleum Exploration and Development*, vol. 46, no. 1, pp. 1–15, 2019.

[6] W. Zhao, Z. Wang, S. Hu, W. Pan, Y. Yang, and H. Bao, "Large-scale hydrocarbon accumulation factors and characteristics of marine carbonate reservoirs in three large onshore cratonic basins in China," *Acta Petrolei Sinica*, vol. 79, no. S2, pp. 195–198, 2012.

[7] L. Jian, W. Zhang, X. Luo, and G. Hu, "Paleokarst reservoirs and gas accumulation in the Jingbian field, Ordos Basin," *Marine and Petroleum Geology*, vol. 25, no. 4-5, pp. 401–415, 2008.

[8] C. N. Zou, C. C. Xu, Z. C. Wang et al., "Geological characteristics and forming conditions of the platform margin large reef-shoal gas province in the Sichuan Basin," *Petroleum Exploration and Development*, vol. 38, no. 6, pp. 641–651, 2011.

[9] L. H. Liu, Y. S. Ma, B. Liu, and C. L. Wang, "Hydrothermal dissolution of Ordovician carbonates rocks and its dissolution mechanism in Tarim Basin, China," *Carbonates and Evaporites*, vol. 32, no. 4, pp. 525–537, 2017.

[10] Y. S. Ma, X. Y. Cai, X. S. Guo, T. L. Guo, and P. R. Zhao, "Polycrystal synthesis and single crystal growth of $CdGeAs_2$," *Journal of Inorganic Materials*, vol. 25, no. 11, pp. 1195–1198, 2010.

[11] X. S. Wei, H. D. Chen, D. F. Zhang, R. Dai, Y. R. Guo, and J. P. Chen, "Gas exploration potential of tight carbonate reservoirs: a case study of Ordovician Majiagou Formation in the eastern Yi-Shan slope, Ordos Basin, NW China," *Petroleum Exploration and Development*, vol. 44, no. 3, pp. 347–357, 2017.

[12] H. Yang, X. S. Liu, and D. F. Zhang, "Sexual behaviour after antiretroviral therapy initiation in female sex workers and HIV-positive patients from the general population, Cotonou, Benin," *Natural Gas Industry*, vol. 25, no. 11, pp. 1426–1432, 2013.

[13] J. Garland, J. Neilson, S. E. Laubach, and K. J. Whidden, "Advances in carbonate exploration and reservoir analysis," *Geological Society, London, Special Publications*, vol. 370, no. 1, pp. 1–15, 2012.

[14] D. Liu, D. Ren, K. Du, Y. Qi, and F. Ye, "Impacts of mineral composition and pore structure on spontaneous imbibition in tight sandstone," *Journal of Petroleum Science and Engineering*, vol. 201, article 108397, 2021.

[15] N. Li, C. W. Xiao, L. H. Wu, Y. J. Shi, H. L. Wu, and Q. F. Feng, "The innovation and development of log evaluation for complex carbonate reservoir in China," *Well Logging Technology*, vol. 38, no. 1, pp. 1–10, 2014.

[16] Q. Wang, Y. Xu, X. S. Liu, D. X. Ma, X. F. Ma, and S. T. Li, "Forming mechanism and main controlling factors on the higlrquality gas reservoirs restricted by paleokarst background: a case from Ordovician $M5_4^1$ carbonate, Ordos Basin," *Natural Gas Geoscience*, vol. 27, no. 12, pp. 2103–2114, 2016.

[17] J. L. Yao, L. P. Wang, Q. Zhang, Z. M. Li, and J. L. Zhang, "Controlling factor and distribution of paleo-karst developmentin Ordovician of southern Ordos Basin," *Natural Gas Geoscience*, vol. 22, no. 1, pp. 56–65, 2011.

[18] W. H. Bai, X. M. Lu, X. J. Li, and W. Wei, "The mode of palaeokarstification and the fine reconstruction of the palaeogeomorphology in the karst basin:taking Ordovician karst in eastern ordos basin for example," *Geoscience*, vol. 16, no. 3, pp. 292–298, 2002.

[19] Z. X. He, C. B. Zheng, A. N. Chen, and Y. F. Wang, "Distributive configuration of ancient valley-trough on Ordovician erosion surface in changing gas field and its control over gas accumulations," *Acta Perolei Sinica*, vol. 15, no. 3, pp. 247–252, 2001.

[20] H. Z. Qu, M. Y. Liu, Y. F. Zhang, Z. Y. Wang, Z. H. Zhang, and S. Y. Li, "Paleokarstic water tables and their control on reservoirs in Ordovician Yingshan Formation, Tazhong Area, Tarim Basin," *NW China.Petroleum Exploration and Development*, vol. 45, no. 5, pp. 817–827, 2018.

[21] H. Liu, T. Ma, X. C. Tan, W. Zeng, G. Hu, and D. Xiao, "Origin of structurally controlled hydrothermal dolomite in epigenetic karst system during shallow burial: an example from Middle Permian Maokou Formation, central Sichuan Basin, SW China," *Petroleum Exploration and Development*, vol. 43, no. 6, pp. 1000–1012, 2016.

[22] D. Z. Chen, "Structure-controlled hydrothermal dolomitization and hydrothermal dolomite reservoirs," *Oil & Gas Geology*, vol. 29, no. 5, pp. 614–622, 2008.

[23] J. S. Huang, H. Shi, M. Zhang, L. C. Shen, J. Liu, and W. H. Wu, "Strontium isotope evolution and global sea-level changes of Carbon;iferous and Permian marine carbonate, Upper Yangtze Platform," *Acta Sedimentologica Sinica*, vol. 19, no. 4, pp. 481–487, 2001.

[24] R. K. Mclimans, "The application of fluid inclusions to migration of oil and diagenesis in petroleum reservoirs," *Applied Geochemistry*, vol. 2, no. 5-6, pp. 585–603, 1987.

[25] X. Q. Li, D. J. Hou, Y. J. Tang, G. Y. Hu, and B. Xiong, "Molecular geochemical evidence for the origin of natural gas from dissolved hydrocarbon in Ordovician Formation waters in Central Ordos Basin," *Chinese Journal of Geochemistry*, vol. 22, no. 3, pp. 193–202, 2003.

[26] S. J. Huang, H. Qing, C. R. Pei, Z. W. Hu, S. J. Wu, and Z. L. Sun, "Strontium concentration, isotope composition and dolomitization fluids in the Feixianguan Formation of Triassic, eastern Sichuan of China," *Acta Petrologica Sinica*, vol. 22, no. 8, pp. 2123–2132, 2006.

[27] J. J. Yang, S. J. Huang, W. Z. Zhang, M. Y. Huang, G. X. Liu, and L. P. Xiao, "Experimental simulation of dissolution for carbonate with different composition under the conditions from epigenesist to burial diagenesis environment," *Acta Sedimentologica Sinica*, vol. 13, no. 4, pp. 49–54, 1995.

[28] M. Fan, K. Hu, X. Q. Jiang, W. X. Liu, J. Y. Zhang, and H. Y. Chen, "Meta-synthesis pattern of analysis and assessment of earthquake disaster system," *Geochemical*, vol. 29, no. 11, pp. 1–18, 2009.

[29] Y. Ming, L. Xu, G. Zhou, H. F. Zhou, Y. Li, and X. Dai, "Evolution characteristics of paleo-karst fracture and vug filling in Maokou Formation, southern Sichuan Basin," *Natural Gas Exploration and Development*, vol. 44, no. 1, pp. 46–54, 2021.

[30] F. H. Xu, H. F. Yuan, G. S. Xu, and X. P. Luo, "Fluid charging and hydrocarbon accumulation in the Cambrian Longwangmiao Formation of Moxi Structure, Sichuan Basin, SW China," *Petroleum Exploration and Development*, vol. 45, no. 3, pp. 426–435, 2018.

[31] G. Q. Wei, Z. Y. Xie, G. L. Bai, J. Li, Z. H. Wang, and A. G. Li, "Organic geochemical characteristics and origin of natural gas in the Sinian-Lower Paleozoic reservoirs," *Sichuan Basin. Natural Gas Industry*, vol. 34, no. 3, pp. 44–49, 2014.

[32] J. Y. Gu, "Characteristics and evolutional model of karst reservoir of Lower Ordovician carbonate rocks in Lunnan area of Tarim Basin," *Journal of Palaeogeography*, vol. 1, no. 1, pp. 54–60, 1999.

[33] X. S. Liu, Y. L. Qi, S. Y. Li, X. Q. Deng, Q. Wang, and W. X. Zhang, "Analysis on the types and the filling process of the gypsum-model pore of $Ma5_4^1$ in northeast of the palaeohigh, Ordos Basin," *Acta Sedimentologica Sinica*, vol. 35, no. 6, pp. 1–10, 2017.